Sensors and Actuators A 226 (2015) 137–142

Contents lists available at ScienceDirect

Sensors and Actuators A: Physical

journal homepage: www.elsevier.com/locate/sna

3D printed molds for non-planar PDMS microfluidic channels

Yongha Hwang[a,*,1], Omeed H. Paydar[b,1], Robert N. Candler[a,c]

[a] Department of Electrical Engineering, University of California, Los Angeles, CA 90095, USA
[b] Biomedical Engineering Interdepartmental Program, University of California, Los Angeles, CA 90095, USA
[c] California NanoSystems Institute, University of California, Los Angeles, CA 90095, USA

ARTICLE INFO

Article history:
Received 8 October 2014
Received in revised form 4 February 2015
Accepted 18 February 2015
Available online 25 February 2015

Keywords:
Three-dimensionally (3D) printing
Arbitrary microchannel geometry
Microfluidics
Polydimethylsiloxane (PDMS)

ABSTRACT

This article introduces the use of three-dimensionally (3D) printed molds for rapid fabrication of complex and arbitrary microchannel geometries that are unattainable through existing soft lithography techniques. The molds are printed directly from computer-aided design (CAD) files, making rapid prototyping of microfluidic devices possible in hours. The resulting 3D printed structures enable precise control of various device geometries, such as the profile of the channel cross-section and variable channel diameters in a single device. We report fabrication of complex 3D channels using these molds with polydimethylsiloxane (PDMS) polymer. Technology limits, including surface roughness, resolution, and replication fidelity are also characterized, demonstrating 100-μm features and sub-micron replication fidelity in PDMS channels.

© 2015 Elsevier B.V. All rights reserved.

1. Introduction

Polymer-based microfluidic devices have revolutionized biomedical research and diagnostics due to the many advantages that elastomers have over rigid materials (e.g., silicon, glass), including fast prototyping, low cost, and gas-permeability for long-term cell viability [1–3]. Polydimethylsiloxane (PDMS) is the most commonly used polymer for microfluidics. PDMS is optically transparent (240–1100 nm), nontoxic, electrically insulating, and impermeable to liquids. Additionally, the PDMS prepolymer conforms to the contours of a mold with high fidelity (~10's nm) [3].

Presently, the fabrication of a mold (or master) requires substrates with positive surface relief structures [4,5], typically a photoresist on silicon wafer, to shape the PDMS prepolymer. Defining these mold microstructures requires cleanroom access, microfabrication tools, extensive training, and expensive reagents. Moreover, this method, based on integrated circuit (IC) fabrication processes, is constrained to planar structures. The simplest three-dimensional (3D) structures require multiple lithography steps, precise layer alignment, and are typically limited to extrusions of two-dimensional (2D) geometries. Consequently, complex 3D structures, including vias [6,7] and multi-tier devices [8], remain a fabrication challenge.

While 3D printed structures cannot *currently* compete with the resolution of structures defined using photolithography, they do enable enhanced control of device geometries, including the profile of the channel cross-section and varying channel heights in a single device. Because of this design flexibility, 3D printed microfluidic technology will give researchers the ability to quickly and inexpensively create channels with unprecedented shape and complexity.

Innovative alternatives to cost-prohibitive microfluidic device fabrication include a high-resolution shrink film device with high aspect ratio (HAR) channels [9] and inkjet-printed devices [10–12]. The shrink film devices can be fabricated to dimensions smaller than their manufacturing resolution due to the shrinking of the film. However, they have not yet been demonstrated with multiple channel heights and full 3D shape control. The inkjet-printed microfluidic devices provide another inexpensive alternative, but are still limited to planar channels defined on the surface of a glass slide. While these solutions do provide a cost-effective approach to microfluidics, possibilities remain for enhancement of 3D microfluidics. For example, a fabrication method with greater control of 3D geometry would allow non-planar channels with continuously variable shape and interwoven structures with unimpeded fluid flow.

3D printing for rapid prototyping has been commercially available for nearly a decade [13]. More recently, advances in 3D printing technology (e.g., non-toxic materials and improved resolution) have enabled scientists and engineers to develop prototypes simply, quickly and cheaply [14–18]. However, 3D printed structures reported so far have been constructed directly from a restricted selection of commercial 3D printing materials, which have

* Corresponding author. Tel.: +1 310 780 3769.
E-mail address: hwangyongha@ucla.edu (Y. Hwang).
[1] These authors contributed equally on this study.

http://dx.doi.org/10.1016/j.sna.2015.02.028
0924-4247/© 2015 Elsevier B.V. All rights reserved.

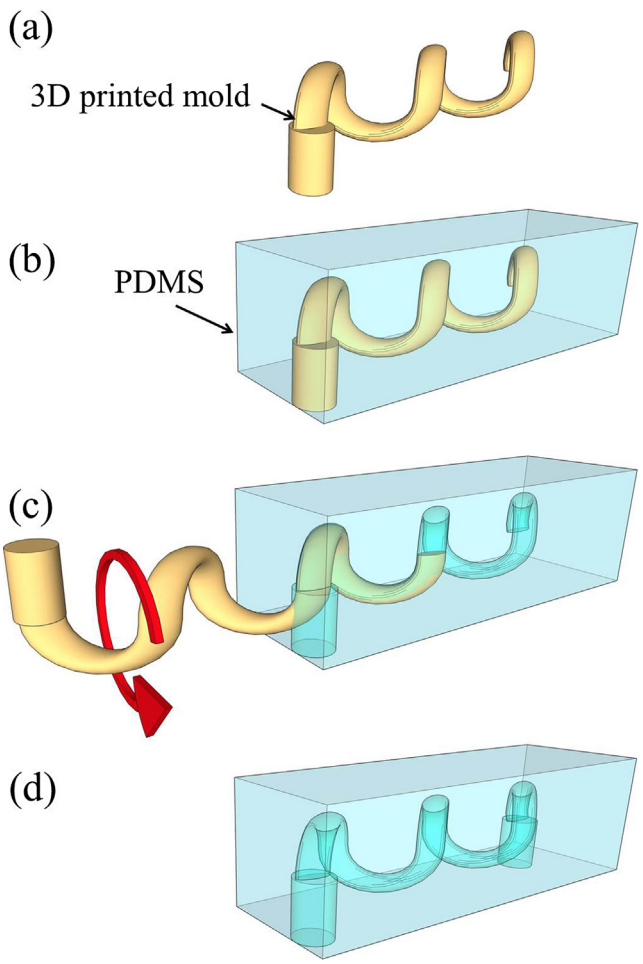

Fig. 1. The fabrication process. (a) The 3D printed mold as fabricated in Fig. 2. (b) PDMS prepolymer poured and cured around the replica mold. (c) Mold extraction after PDMS is cured, accomplished by rotating the mold. (d) Complete non-planar PDMS microfluidic channel.

limitations when compared to PDMS (e.g., biocompatibility, permeability to gas for cell viability, and optical transparency). We propose, for the first time, rapid prototyping of structures that can be used to mold PDMS microchannels with hundreds of microns resolution and nearly arbitrary topography (e.g., variable channel height and cross-section) as illustrated in Fig. 1. The ability to design arbitrary channel heights could open up new design spaces for microfluidic devices, such as biomimetic channels that reproduce the exact shape of blood vessels.

In addition to the technical advantages, this economical alternative can help accelerate research progress by increasing access to a once-limited field. In addition, unlike conventional microfluidic device fabrication where increasing the number of channel layers quickly becomes prohibitively complex, the fabrication of 3D printed master-molds for multi-tier devices is no more difficult than the fabrication of simple 2D geometries.

2. Materials and methods

2.1. Design, print, and pour

Microchannel molds are printed directly (Objet24, Stratasys, Eden Prairie, MN, USA) from computer-aided design (CAD) files (Autodesk Inventor, Autodesk, Inc., San Rafael, CA, USA). The fully automated printing process simultaneously jets a photocurable polymer and a support material in ~28-μm layers (Fig. 2); a typical

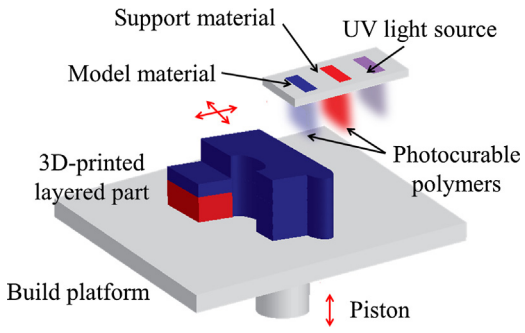

Fig. 2. Three-dimensional (3D) printing process using the Objet24 printer. Model (blue) and support (red) photopolymers are dispensed and immediately UV-cured in ~28-μm layers. The gel-like support material is removed with pressurized water, revealing the final device. The resolution limit of this printer is 600 × 600 × 900 dpi (dots per inch)—ideally capable of 45 μm line widths. (For interpretation of the references to color in this figure legend, the reader is referred to the web version of this article.)

mold of 50 mm × 50 mm × 5 mm takes approximately 30 min to print. Each layer of the model and support material is immediately UV-cured. Upon completion of the printing process, a high-pressure water jet exposes the final device design by dissolving the support material. The 3D printed device becomes the replica mold. The model material (Objet VeroWhitePlus RGD835) and support material (Objet Support SUP705) were purchased from Stratasys and used as received [19].

A base-to-catalyst mixture (9.1% w/w) of silicone elastomer (PDMS, Sylgard 184, Dow Corning, Midland, MI, USA) was poured onto the master, desiccated, and cured at 75 °C. The device was removed from the mold as shown in Fig. 1 (also see video in supplementary information).

2.2. Characterization

Because PDMS conforms to the contours of the mold with high fidelity, it is important to characterize the surface topology of the 3D printed mold itself. The resolution of printed molds can be limited by droplet size of model material, 3D printer nozzle spacing, and reflow of model material prior to UV curing. To investigate these limitations, surface roughness of 3D printed samples (2 mm × 1.25 mm) was quantified and compared to surface roughness measurements of conventional replica-mold materials, silicon and photoresist (SU-8). The printer provides two options for surface finish, glossy and matte, both of which were characterized. The matte finish results on surfaces where the printed material is in contact with support material.

The surface roughness measurements were taken with an optical profiler (Wyko NT3300, Veeco, Fullerton, CA, USA). Vertical scanning interferometry (VSI) resolves the surface topography by detecting the interference between emitted light and the reflected beam. 3D printed samples that were imaged with VSI were sputter coated with a 100-Angstrom layer of chromium/gold for improved reflectivity and image quality. The average of the absolute value of deviation from the mean surface height is used as a measure of the surface roughness, R_a.

The 3D printing process was used to fabricate two types of structures: characterization devices (e.g., roughness test structures, periodic pillars) and demonstration devices (e.g., variable diameter double helices). The periodic pillars, which have the same diameters but different pitch, were printed to test effective resolution of the printed molds. The resolution is primarily limited by droplet spreading of the 3D printer. The double helical molds were used to fabricate PDMS channels with arbitrary control of 3D geometry.

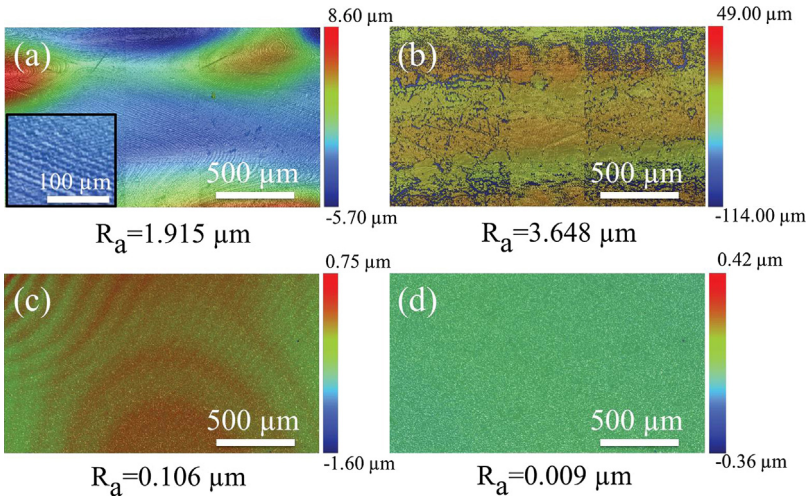

Fig. 3. Vertical scanning interferometry (VSI) of microfluidic model materials. (a) The glossy and (b) matte 3D printed surface roughness, R_a, is an order of magnitude larger than (c) the channel-defining SU-8 feature. (d) Silicon is also shown. Inset of (a) is magnified four times to show periodic minima and maxima of the glossy 3D printed surface. All dimensions are given in micrometers.

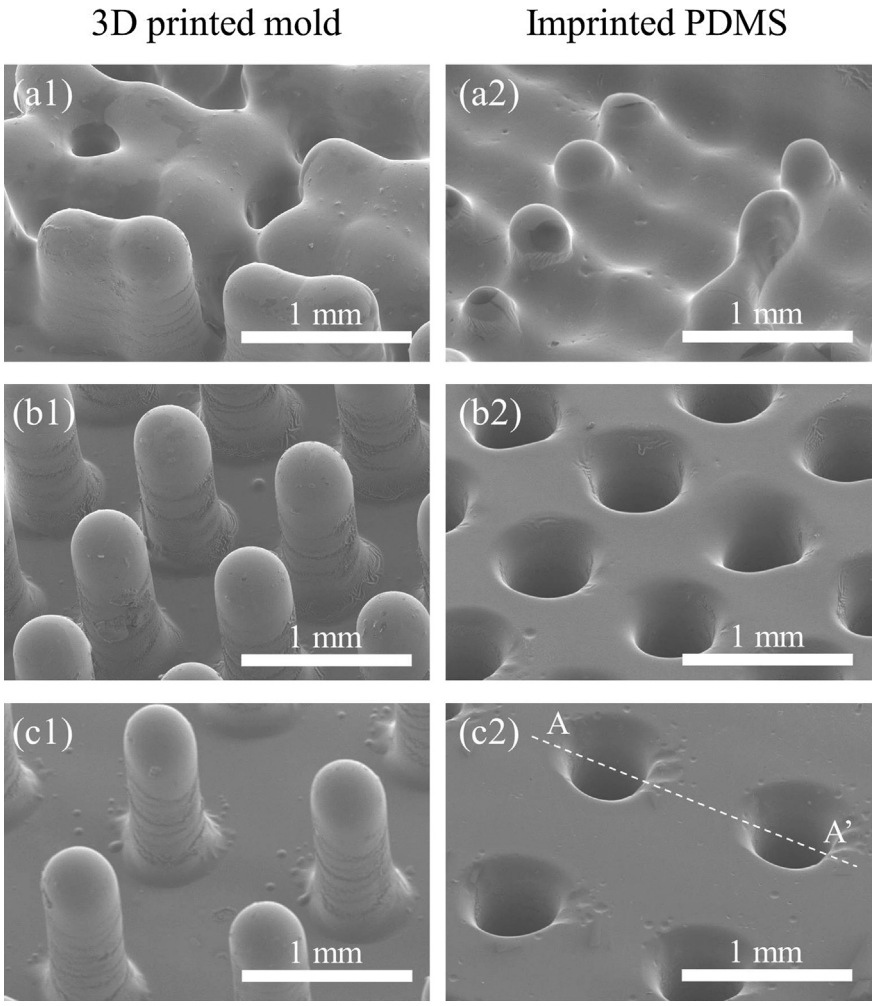

Fig. 4. Pillars designed with 250-µm diameters and 1500-µm heights were printed (left column) and imprinted in PDMS prepolymer (right column) in a rectangular array. The center-to-center spacing was designed to be ((a1) and (a2)) 500 µm, ((b1) and (b2)) 750 µm, and ((c1) and (c2)) 1000 µm. The resulting pillar diameter was measured to be 378 µm due to reflow during the printing process, causing pillars to bleed into one another ((a1) and (a2)).

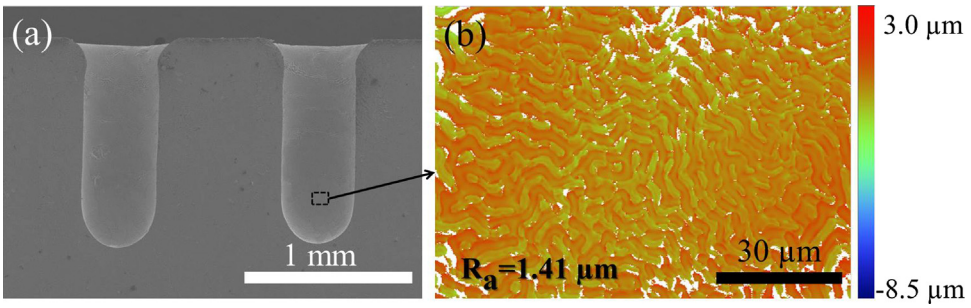

Fig. 5. Cavities designed to have 250-μm diameter, 1500-μm height, and 1000-μm pitch were imprinted in PDMS prepolymer (Fig. 4c2). (a) Cross-section SEM image along AA' in Fig. 4(c2). (b) Vertical scanning interferometry (VSI) of the interior surface of the cavity. A color map is representative of the surface topography. (For interpretation of the references to color in this figure legend, the reader is referred to the web version of this article.)

3. Results and discussion

3.1. Surface roughness of 3D printed structures

3D printed devices, regardless of surface finish, have predictably rougher surface topology than traditional microfluidic molds (Fig. 3). Because microfluidic channels are molded from photoresist relief structures, we compared the roughness of the SU-8 sample with the 3D printed material. Although the surface roughness values of both matte and glossy samples were an order of magnitude larger than conventional microfabricated templates, the surface of the glossy samples is smoother than the matte samples. Therefore, all the structures hereafter were printed with the glossy finished surface.

Fortunately, the periodic minima and maxima (Fig. 3(a))—a consequence of the jetting process—that define the surface topology have not been observed to affect the ability of the PDMS device to bond to glass as a handling substrate, likely due to the low elastic modulus and accompanying conformality of PDMS.

3.2. Resolution of 3D printed devices

Droplet spreading affects the final device dimensions [20]; extruded features print larger than designed (Figs. 4–6). This, however, can be compensated by adjusting the dimensions of the design in anticipation of reflow during the 3D printing process. The initial droplet size and amount of reflow will vary for different printer models, but the results in Figs. 4–6 give a representative range of achievable size scales for Photojet 3D printers. Large arrays of 250-μm diameter pillars were printed with 500 μm, 750 μm, and 1000 μm pitch spacing (Fig. 4). Due to the unintended reflow, the final printed pillar diameters were 378 μm on average, resulting in structures with multiple pillars bleeding into one another when the pitch was not large enough to compensate for the droplet spread. Fig. 4 compares 3D printed molds with PDMS structures created from those molds. Fig. 5 shows the surface roughness of the sidewall of a PDMS cavity created from a 3D printed mold. As can be seen by comparing Figs. 3 and 5, the surface roughness of an imprinted cavity in the PDMS (Fig. 5) was in the same range as the surface roughness of the 3D printed mold (Fig. 3).

Fig. 6, along with Tables S1 and S2 in the supplementary information, describes the designed vs. achieved size of 3D printed pillars and holes. Although they were designed to be 2 mm long, pillars smaller than 200 μm diameters were shorter than 1 mm. 3D printed pillars were wider than designed due to droplet spreading (Fig. 6). As the design shrinks, the relative discrepancy between the designed and printed structures increases. Pillars with less than 40 μm in diameter were not printed at all because the minimum resolution of the 3D printer is 45 μm. Irregular ellipse shapes were printed when designed below 100 μm in diameter. The same analysis was performed for 3D printed holes (see Table S2 in the supplementary information). Holes designed below 400 μm in diameter were not formed due to reflow during the printing process. In general, for the same dimensions, 3D printed pillars resolved better than holes.

3.3. 3D printed double helical channel

Fig. 7 shows one application of the 3D printing technique, where a double helix channel has been fabricated in PDMS (See supplementary video). Each strand of the double helix structure was designed in CAD as a variable diameter channel (500–1000 μm) with a 5-mm pitch (Fig. 7(a) and (e)). The strands were anchored through posts on both ends, and their inner surfaces were separated by 2 mm through the posts on both ends. The PDMS prepolymer was cast around the double helix structure, and the mold was manually extracted following the curing process to create helical channels (Fig. 7(b) and supplementary video). The mold material was observed to inhibit full curing of the PDMS at the mold/PDMS interface. This uncured PDMS at the mold interface actually assists with removal of mold, and the PDMS fully cures after removal of the mold. For illustration purposes, a single channel was filled with dye (Fig. 7(c)). The second channel was then filled with different colored dye to emphasize the ability to create over- and underpasses (Fig. 7(d)). Although the printed device was ~23% larger than designed (Fig. 7(e) and (f)), the PDMS channel (Fig. 7(g)) resembles the teardrop cross-section designed in CAD software.

By controlling design parameters (e.g., channel diameter, shape, and location) we can create arbitrary 3D fluidic networks. Structures with over- and underpasses are difficult with conventional cleanroom processes, but can be designed and printed as

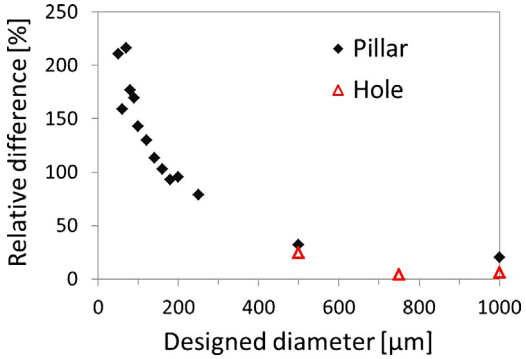

Fig. 6. Relative difference of diameters of 3D printed pillars and holes with comparison to designed dimensions. Pillars with less than 40 μm in diameter and holes with less than 400 μm in diameter were not printed at all because of the minimum resolution and reflow of the 3D printer. Each top-view SEM image comparing the designed with 3D printed shapes is shown on Table S2 of supplementary information.

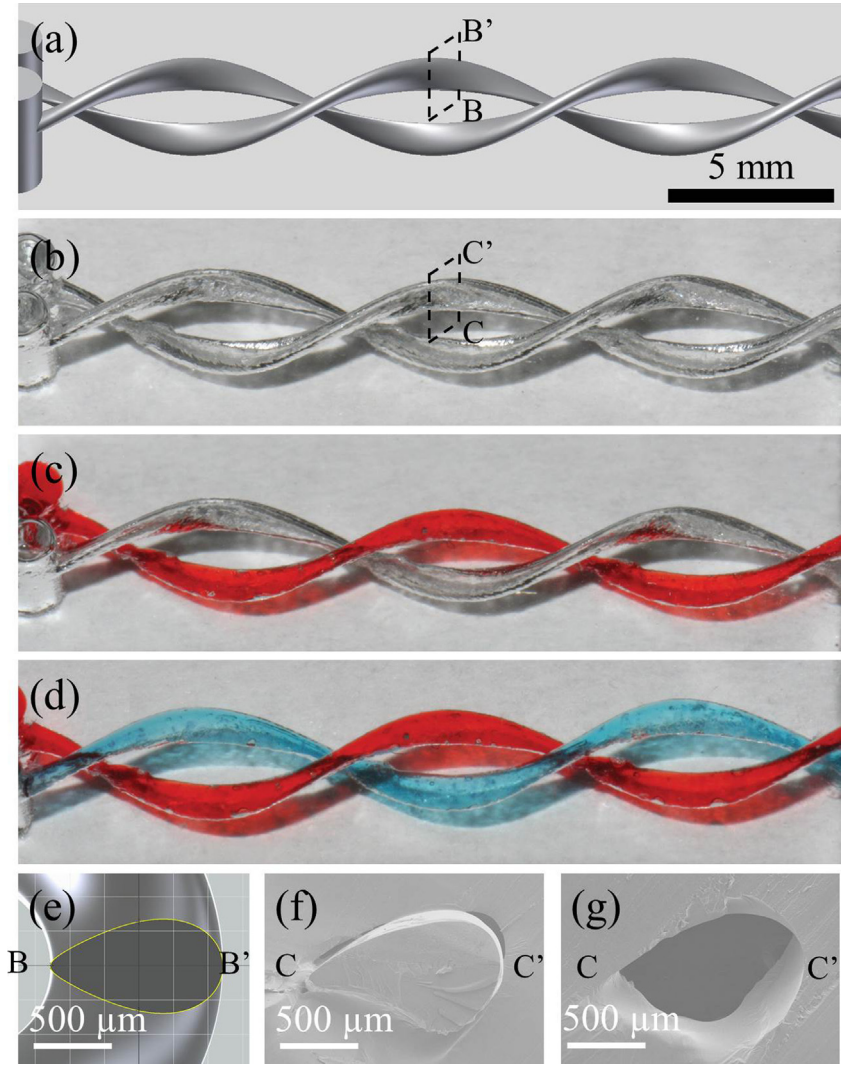

Fig. 7. Variable channel diameter, double-helix structure. (a) Computer-aided design (CAD) schematic used to generate 3D printed mold. (b) PDMS scaffold after removal of 3D printed mold. (c) Single channel with colored water. (d) Both channels filled. (e) CAD schematic of cross-section of one helix taken through BB'. (f) and (g) SEM images of cross-section of one helix channel taken through CC' before and after removal of 3D printed mold, respectively. (For interpretation of the references to color in this figure legend, the reader is referred to the web version of this article.)

interwoven structures and molded in a single PDMS slab without sandwiching or bonding. In addition, the interwoven structure avoids abrupt changes in direction, which are typical of conventional PDMS mold fabrication [6], allowing the fluid to flow unimpeded without static zones of no flow.

Of particular importance, the device in Fig. 7 was fully defined in the PDMS polymer. For conventional PDMS mold fabrication, three sides of the channel are composed of PDMS, while the final side is typically a glass substrate [21]. The devices shown in Fig. 7 have a channel surface that is entirely PDMS, which is beneficial for uniform gas permeability and adhesion in biological applications. This molding technique allows the user to bypass O_2 plasma treatment and avoid bonding the device to glass, which further simplifies the device manufacturing process. However, without oxygen plasma treatment, the untreated PDMS remains hydrophobic (109°) and obstructs fluid flow. To overcome this potential challenge the device can be submerged in 1 M NaOH for 24 h. The resulting surface treatment is more stable than radio-frequency plasma or corona discharge and relieves the flow obstruction of native PDMS [22].

4. Conclusion

3D printed molds for fabrication of PDMS channels were described, demonstrating variable channel dimensions as small as 100s of micrometers in all-PDMS channels. A double helix, variable cross-section channel was fabricated in PDMS as a demonstration of a geometry that would be difficult to achieve via traditional soft lithography processes. We characterized the roughness and resolution of 3D printed materials and investigated the fidelity with which mold patterns can be reliably transferred to PDMS. 3D printed molds could lead to complex three-dimensional PDMS microfluidic networks with unprecedented control of channel geometry.

Acknowledgements

The authors would like to thank the Nanoelectronics Research Facility (NRF) at UCLA for making device characterization possible. This work was partially supported by NSF Grant No. 0926228.

Appendix A. Supplementary data

Supplementary data associated with this article can be found, in the online version, at http://dx.doi.org/10.1016/j.sna.2015.02.028.

References

[1] A. Mata, A.J. Fleischman, S. Roy, Characterization of polydimethylsiloxane (PDMS) properties for biomedical micro/nanosystems, Biomed. Microdevices 7 (2005) 281–293.
[2] J.C. McDonald, D.C. Duffy, J.R. Anderson, D.T. Chiu, H. Wu, O.J.A. Schueller, et al., Fabrication of microfluidic systems in poly (dimethylsiloxane), Electrophoresis 21 (2000) 27–40.
[3] J.C. McDonald, G.M. Whitesides, Poly(dimethylsiloxane) as a material for fabricating microfluidic devices, Acc. Chem. Res. 35 (2002) 491–499.
[4] C.S. Effenhauser, G.J.M. Bruin, A. Paulus, M. Ehrat, Integrated capillary electrophoresis on flexible silicone microdevices: analysis of DNA restriction fragments and detection of single DNA molecules on microchips, Anal. Chem. (1997) 3451–3457.
[5] Y. Xia, G.M. Whitesides, Soft lithography, Angew. Chem. Int. Ed. (1998) 550–575.
[6] C. Carlborg, T. Haraldsson, M. Cornaglia, G. Stemme, W. van der Wijngaart, A high-yield process for 3-D large-scale integrated microfluidic networks in PDMS, J. Microelectromech. Syst. 19 (2010) 1050–1057.
[7] J.R. Anderson, D.T. Chiu, R.J. Jackman, O. Cherniavskaya, J.C. McDonald, H. Wu, et al., Fabrication of topologically complex three-dimensional microfluidic systems in PDMS by rapid prototyping, Anal. Chem. 72 (2000) 3158–3164.
[8] M.A. Unger, H.-P. Chou, T. Thorsen, A. Scherer, S.R. Quake, Monolithic microfabricated valves and pumps by multilayer soft lithography, Science 288 (2000) 113–116.
[9] D. Taylor, D. Dyer, V. Lew, M. Khine, Shrink film patterning by craft cutter: complete plastic chips with high resolution/high-aspect ratio channel, Lab Chip 10 (2010) 2472.
[10] M. Watanabe, Refreshable microfluidic channels constructed using an inkjet printer, Sens. Actuators B: Chem. 122 (2007) 141–147.
[11] M. Watanabe, Microfluidic devices easily created using an office inkjet printer, Microfluid. Nanofluid. 8 (2009) 403–408.
[12] M. Watanabe, An inkjet-printed microfluidic device for liquid–liquid extraction, Analyst 136 (2011) 1420.
[13] B.C. Gross, J.L. Erkal, S.Y. Lockwood, C.P. Chen, D.M. Spence, Evaluation of 3D printing and its potential impact on biotechnology and the chemical sciences, Anal. Chem. 86 (2014) 3240–3253.
[14] M.D. Symes, P.J. Kitson, J. Yan, C.J. Richmond, G.J.T. Cooper, R.W. Bowman, et al., Integrated 3D-printed reactionware for chemical synthesis and analysis, Nat. Chem. 4 (2012) 349–354.
[15] M.S. Mannoor, Z.W. Jiang, T. James, Y.L. Kong, K.A. Malatesta, W.O. Soboyejo, et al., 3D printed bionic ears, Nano Lett. 13 (2013) 2634–2639.
[16] K.G. Lee, K.J. Park, S. Seok, S. Shin, D.H. Kim, J.Y. Park, et al., 3D printed modules for integrated microfluidic devices, RSC Adv. 4 (2014) 32876–32880.
[17] C.K. Su, S.C. Hsia, Y.C. Sun, Three-dimensional printed sample load/inject valves enabling online monitoring of extracellular calcium and zinc ions in living rat brains, Anal. Chim. Acta 838 (2014) 58–63.
[18] J. O'Connor, J. Punch, N. Jeffers, J. Stafford, A dimensional comparison between embedded 3D-printed and silicon microchannels, J. Phys. Conf. Ser. 525 (2014).
[19] Material Safety Data, http://www.stratasys.com/materials/material-safety-data-sheets
[20] F. Tavakoli, S.H. Davis, H.P. Kavehpour, Spreading and arrest of a molten liquid on cold substrates, Langmuir 30 (2014) 10151–10155.
[21] H.K. Wu, B. Huang, R.N. Zare, Construction of microfluidic chips using polydimethylsiloxane for adhesive bonding, Lab Chip 5 (2005) 1393–1398.
[22] I. Hoek, F. Tho, W.M. Arnold, Sodium hydroxide treatment of PDMS based microfluidic devices, Lab Chip 10 (2010) 2283–2285.

Biographies

Yongha Hwang received both the B.S. and M.S. degrees from Electrical Engineering Department in Korea University, Seoul, Korea in 2004 and 2006, respectively. He received the Ph.D. degree in Department of Electrical Engineering from University of California, Los Angeles, CA in 2021. Currently he is a postdoctoral researcher in Sensors and Technology Laboratory, Department of Electrical Engineering, UCLA. His research interestsinclude design, fabrication and characterization of nano- and microelectromechanical systems for sensor and actuator applications, including 3D printed materials for microfluidics, energy dissipation mechanisms in low frequency resonant structures, and micromechanical resonators and mirrors for chemical/biomedical sensing.

Omeed H. Paydar graduated from Purdue University in 2008 with a B.S. in Biomedical Engineering and is currently a Ph.D. candidate in Biomedical Engineering at the University of California, Los Angeles. While at UCLA, Omeed has begun to develop a technical expertise in microelectromechanical systems (MEMS). His research includes fabrication of neural probes, development of tactile sensors for minimally invasive surgical systems, and design of miniature, custom MRI coils for clinicians.

Robert N. Candler received the B.S. in Electrical Engineering from Auburn University in 2000, and he received the M.S. and Ph.D. in Electrical Engineering from Stanford University as an NDSEG and NSF Fellow in 2002 and 2006, respectively. He is currently an Assistant Professor of Electrical Engineering University of California, Los Angeles with a joint appointment in the California NanoSystems Institute. He also serves as the Faculty Director of the Nanoelectronics Research Facility (NRF), a multi-user nanofabrication facility. Prof. Candler's research expertise is in micro- and nano-electromechanical systems (MEMS/NEMS), including microscale magnetic devices for electron beam manipulation, the fundamental behavior of MEMS/NEMS resonators, sensing systems for surgical tools, and multiferroics. He was awarded the Young Investigator Award from the Army Research Office and the Northrop Grumman Excellence in Teaching Award from the UCLA Henry Samueli School of Engineering and Applied Sciences, both in 2012. He also received the NSF CAREER Award in 2014. Before coming to UCLA, he spent three years in Corporate R&D at the Bosch Research and Technology Center, serving concurrently as a consulting assistant professor at Stanford University with the Departments of Electrical and Mechanical Engineering. He has authored or co-authored more than 50 papers in major conferences and journals, three book chapters, and four patents.